energies

MDPI

Article

Maximum Power Point Tracking of Photovoltaic Module Arrays Based on a Modified Gray Wolf Optimization Algorithm

Kuo-Hua Huang, Kuei-Hsiang Chao *, Ying-Piao Kuo and Hong-Han Chen

Department of Electrical Engineering, National Chin-Yi University of Technology, Taichung 41170, Taiwan; huangkh@ncut.edu.tw (K.-H.H.); kuoyp@ncut.edu.tw (Y.-P.K.); danjor0709@gmail.com (H.-H.C.)
* Correspondence: chaokh@ncut.edu.tw; Tel.: +886-4-2392-4505 (ext. 7272); Fax: +886-4-2392-2156

Abstract: In this study, a modified gray wolf optimization algorithm (GWOA) was proposed to facilitate the maximum power point tracking (MPPT) of photovoltaic module arrays (PMAs). To increase the voltage conversion ratio and achieve a voltage boost through reduced duty cycles, a high-voltage step-up converter with a coupled inductor was used to replace the conventional energy storage inductor. To achieve global MPPT, the iteration parameters of the proposed GWOA were adjusted according to the slope of the PMA power–voltage (P–V) curve. According to the simulation results, the modified GWOA is more effective in MPPT than the perturbation and observation algorithm and conventional GWOA when multiple peaks appear in the P–V curve of a shaded PMA. In addition, the modified GWOA exhibits an improved tracking speed response and steady-state response.

Keywords: gray wolf optimization algorithm; photovoltaic module array; global maximum power point tracking; partial shading; coupled inductor; high-voltage step-up converter

check for updates

Citation: Huang, K.-H.; Chao, K.-H.; Kuo, Y.-P.; Chen, H.-H. Maximum Power Point Tracking of Photovoltaic Module Arrays Based on a Modified Gray Wolf Optimization Algorithm. *Energies* **2023**, *16*, 4329. https://doi.org/10.3390/en16114329

Academic Editor: Guojiang Xiong

Received: 4 April 2023
Revised: 10 May 2023
Accepted: 23 May 2023
Published: 25 May 2023

1. Introduction

Countries worldwide have continued to promote renewable energy sources, among which photovoltaic power generation is regarded as one of the most crucial technologies. Changes in irradiation intensity and temperature result in nonlinear variations in the power–voltage (P–V) curves of photovoltaic module arrays (PMAs). Therefore, to maintain the operation of PMAs at the maximum power point (MPP) under all conditions, the maximum power point tracking (MPPT) technique must be used. Among the conventional MPPT methods commonly used in practice are perturbation and observation (P&O), power feedback, voltage feedback, and incremental conductance [1,2]. P&O algorithms are particularly advantageous because of their simple structure and limited measurement parameters. However, these algorithms are relatively inaccurate, and their solutions tend to oscillate near the MPP. Conventional P&O algorithms can track MPPs only when the PMA P–V curve exhibits a single peak. When a PMA malfunctions or becomes shaded, its P–V curve generates multiple peaks, which trap the algorithm in a local maximum and prevent it from identifying the global maximum.

Many researchers have proposed various smart MPPT methods to address multipeak P–V curves [3] generated by partially shaded PMAs [4–15]. Among the commonly used smart MPPT methods are ant colony optimization [5,6], artificial bee colony algorithms [7,8], particle swarm optimization [9,10], genetic algorithms [11], teaching–learning-based optimization [12], and cuckoo search-learning-based optimization [13–15]. Ant colony optimization is a probabilistic technique used for identifying optimization paths. It involves a simple framework and entails the configuration of certain parameters at the cost of a slow search process [5,6]. Although artificial bee colony algorithms require few parameters and converge rapidly, their tracking speed and stability are affected by the number of scout bees and may result in an excessively long tracking speed response [7,8]. Compared with other

methods, particle swarm optimization requires a small number of evolutionary swarms. However, it easily falls into local maxima, thereby producing inaccurate results [9,10]. In genetic algorithms, parameters are encoded and converted into genetic formats to identify optimal solutions through evolutionary calculations [11]. These algorithms address multiple points in a space instead of focusing on a single point to avoid being trapped in a local maximum. Therefore, genetic algorithms are effective in identifying optimal solutions while maintaining a low convergence rate. However, when genetic algorithms are used independently, the computation required for a large population may result in an excessively long tracking time. Similar to particle swarm optimization, teaching–learning-based optimization uses a scatter search and memory-based approach [12]. This technique can be used to perform continuous and complex searches and entails the configuration of only a few parameters. Because its principle is easy to understand, teaching–learning-based optimization has been extensively used in system optimization. However, because each learner has variable performance, the limited range of parameters (i.e., teaching factors) may result in the use of inappropriate parameters, thereby causing poor learning outcomes and an excessively long tracking response. Cuckoo search-learning-based optimization is a swarm intelligence algorithm proposed by Yang and Deb et al. in 2009 [13–15]. This algorithm is based on the brood parasitism of cuckoo birds and the Levy flight behavior of certain animal species. A Levy flight is a random walk process in which random numbers are generated through a Levy distribution. The random walk process is used to select nests, update the nest location, and solve optimization problems by identifying the global optimal nest location. In conventional cuckoo search-learning-based optimization, the step length is fixed within the upper and lower limits of the step factor to track the global MPP. Consequently, this technique requires an extended amount of time to complete the tracking process. In addition, the solution tends to oscillate near the global MPP, which prevents the technique from improving the transient and steady-state response of the MPP tracker.

Other researchers have explored the integration of smart algorithms and conventional MPPT techniques [16,17] by combining particle swarm optimization with genetic algorithms and P&O algorithms. However, although this approach can help identify the global optimal solution, its tracking speed response requires further improvement. Bayesian optimization algorithm (BOA) is an optimization algorithm based on Bayes' theorem [18]. This algorithm generally requires a lot of computational resources and time because it requires a lot of function evaluation and Bayesian inference while also being highly sensitive to the initial values, so it requires an appropriate selection of the initial values to find the optimum solution. The algorithm is difficult to use and adjust because it needs to adjust several parameters, such as the compute kernel and the prior probability. In addition, the Bayesian optimization algorithm also has special requirements for the target function, which must be both continuous and differentiable, and the convergence rate is slow when dealing with non-smooth or multi-peaked functions.

In this study, a modified gray wolf optimization algorithm (GWOA) based on conventional GWOA [19–23] was proposed to track the MPP of PMAs. Even when multiple peaks appear on the P–V curve of a malfunctioning or shaded PMA, the proposed algorithm can rapidly track the global MPP. Compared with conventional P&O algorithms and GWOAs, the proposed modified algorithm offers a faster tracking speed response and steady-state response.

2. Properties of PMAs

In photovoltaic power generation systems, PMAs comprise multiple modules connected in parallel and series. In these systems, environmental conditions such as shading by tall trees, buildings, clouds, dust, and dirt reduce the output power of PMAs and cause their P–V curves to generate multiple peaks. In this study, to examine the characteristics of shaded PMAs, a PMA composed of three parallel strings, with each string containing four SWM-20W photovoltaic power generation modules (Dongguan, China) connected in series, was examined. Table 1 lists the electrical specifications of the SWM-20W module [18].

Figure 1 depicts the current–voltage (I–V) and power–voltage (P–V) curves of the PMA simulated using MATLAB at different levels of irradiation intensity at 25 °C. Figure 2 shows the I–V and P–V curves when a single module in two different strings was affected by varying levels of shading. Under these conditions, the P–V curve exhibited multiple peaks. Figure 3 depicts the architecture of the MPPT controller based on the modified GWOA.

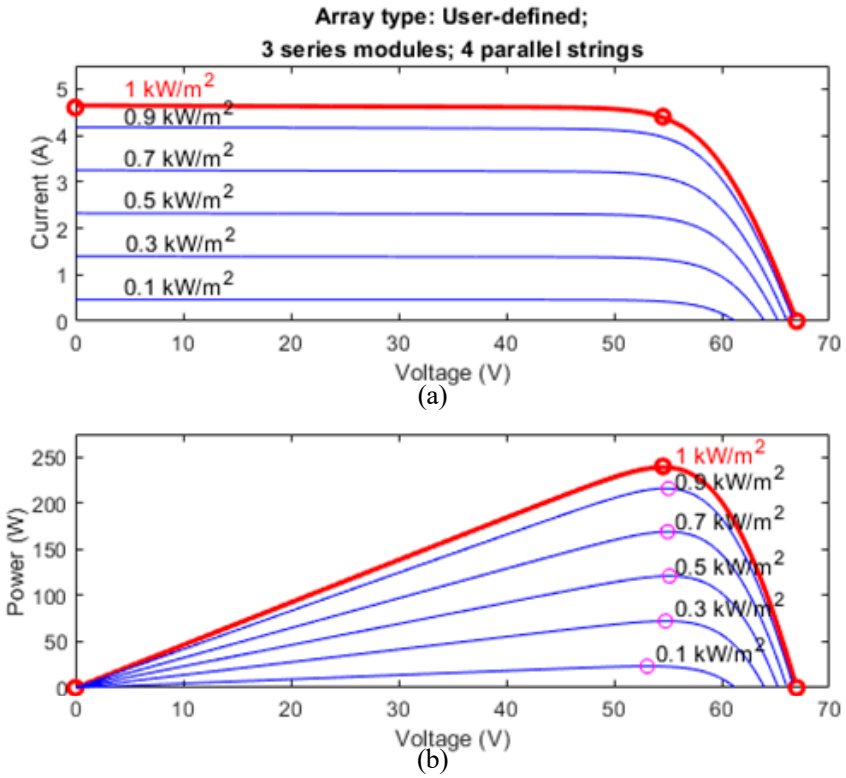

Figure 1. Characteristics of the PMA at different levels of irradiation intensity at 25 °C: (**a**) I–V curves and (**b**) P–V curves.

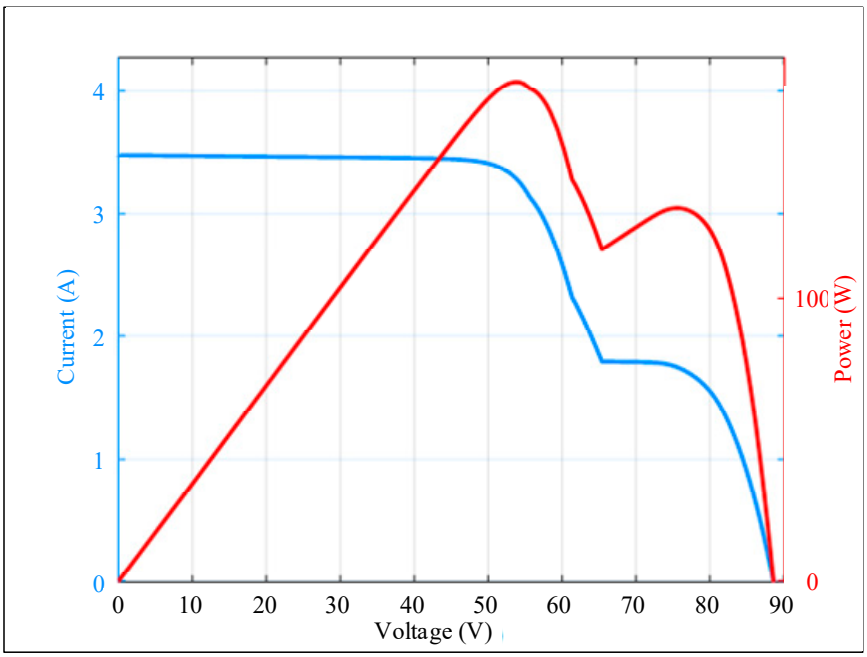

Figure 2. I–V (blue line) and P–V (red line) curves of the PMA when a single module in two different strings was affected by varying levels of shading.

Table 1. Electrical specifications of the SWM-20W module [24].

Parameter	Value
Maximum output power (P_{max})	20 W
MPP current (I_{MPP})	1.10 A
MPP voltage (V_{MPP})	18.18 V
Short-circuit current (I_{SC})	1.15 A
Open-circuit voltage (V_{OC})	22.32 V

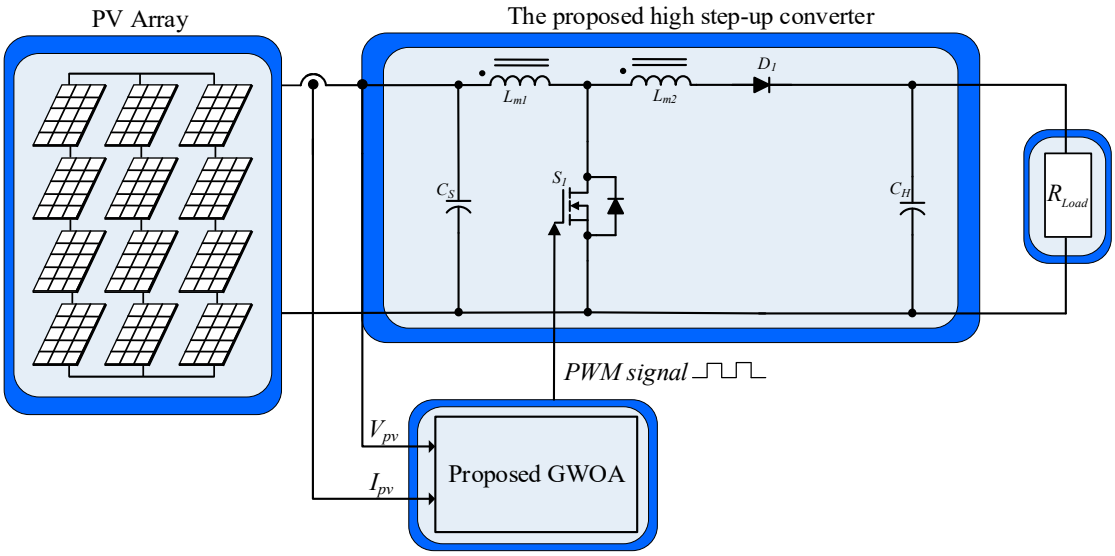

Figure 3. Architecture of the MPPT controller based on the modified GWOA.

3. GWOA

In 2014, Seyrdali Mirjalili, Seyed Mohammad Mirjalili, and Andrew Lewis proposed the GWOA [19–23]. This algorithm mimics the social hierarchy and hunting behavior of gray wolves in nature. The hunting process is divided into three stages: surrounding, following, and prey hunting. When iterations of the hunting process are completed by gray wolf populations of different hierarchical levels, the wolves in the highest hierarchical level are continuously updated to identify the global optimal solution.

3.1. Conventional GWOA

The following are the computational steps of the conventional GWOA.

Step 1: The number of wolves n_T and the maximum iteration number i_{max} are configured, and the optimization parameters B, K, and α and the fitness value of each wolf are initialized.

Step 2: The locations of the top three wolves with the largest fitness values are set as Y_a, Y_b, and Y_c, with Y_a, which denotes the location of the top wolf, being the current optimal solution.

Step 3: Equation (1) is used to calculate the random distance between the location $Y(i)$ of each remaining wolf n and the locations of the top three wolves (i.e., Y_a, Y_b, and Y_c), and Equations (2) and (3) are then used to update the location (i.e., fitness value) of each wolf n:

$$\begin{cases} d_a(i) = |K \cdot Y_a(i) - Y(i)| \\ d_b(i) = |K \cdot Y_b(i) - Y(i)| \\ d_c(i) = |K \cdot Y_c(i) - Y(i)| \end{cases} \quad (1)$$

$$\begin{cases} Y_1(i+1) = Y_a(i) - B \cdot d_a(i) \\ Y_2(i+1) = Y_b(i) - B \cdot d_b(i) \\ Y_3(i+1) = Y_c(i) - B \cdot d_c(i) \end{cases} \quad (2)$$

$$Y_m(i+1) = [Y_1(i+1) + Y_2(i+1) + Y_3(i+1)]/3 \quad (3)$$

where B and K are iteration parameters; $d_a(i)$, $d_b(i)$, and $d_c(i)$ are the random distances between the locations of the top three wolves (a, b, and c) and the location of each remaining wolf n; $Y(i)$ is the current location of each wolf n; $Y_1(i+1)$, $Y_2(i+1)$, and $Y_3(i+1)$ represent the updated location of each wolf n relative to the locations of the top three wolves; and $Y_m(i+1)$ is the mean of the updated location (i.e., the new fitness value) of each wolf n.

Step 4: Equations (4) and (5) are used to update the parameters B, K, and α:

$$B = 2\alpha \cdot r_1 - \alpha \quad (4)$$

$$K = 2 \cdot r_2 \quad (5)$$

where α decreases linearly from 2 to 0 as the number of iterations increases, and r_1 and r_2 are random values in the closed interval [0, 1].

Step 5: When the iteration number reaches the preset maximum iteration number, the iteration process is terminated to record the top three fitness values (Y_a, Y_b, and Y_c), and the optimal fitness value Y_a is output. If the preset conditions are not met, then the calculation process is repeated from Step 2.

3.2. Modified GWOA

As a result of its multiple strengths, including its straightforward principle, high search speed, high search accuracy, and ease of implementation, the GWOA is regarded as a highly valuable technique. However, this smart algorithm is still relatively new, and its research is still in its infancy. Therefore, the theoretical foundation and evolution of the GWOA require further investigation. In this study, to enhance the functionality of the GWOA, a modified GWOA was proposed by relying on Equation (6) to adjust α. This approach facilitates the use of large step lengths in early iterations to identify the optimal solution. Subsequently, the criteria listed in Table 2 were used to slightly adjust α with respect to changes in the slope of the P–V curve, thereby avoiding local maxima and identifying the global optimal solution. According to Table 2, α must be adjusted only when $\Delta P > 0$ because an adjustment to α increases the output power of the PMA under this condition such that the adjustment in the following iteration would accelerate the MPPT. Figure 4 presents the trend of α with respect to the number of iterations and slope of the P–V curve. Figure 5 depicts the relationship between the slope s of the P–V curve and changes in the PMA output power ΔP. Figure 6 shows a flowchart of the modified GWOA's iteration process.

$$\Delta\alpha = \alpha_o - \left[\alpha_o \times \left(\frac{i}{i_{\max}}\right)^2\right] \quad (6)$$

where $i_{\max}$ is the maximum iteration number (which was set to 50 in this study), i is the current iteration number, and α_o is the initial iteration parameter (which was set to 2 in this study).

The conventional GWOA and the proposed modified GWOA are set with the number of gray wolves n_T = 5, the maximum iteration of $i_{\max}$ = 50, and the iteration parameters B, K, and α. The iterative equations are shown in Equations (4)–(6), respectively. The maximum output power of the photovoltaic module array varies under different sunlight, temperature, and shading conditions. As a result, the number of iterations needed to track the global maximum power point will be different, and the global maximum power point is not known in advance. Therefore, in this paper, the total number of iterations of the algorithm is set to a larger number of iterations, $i_{\max}$ = 50, to ensure that all methods can track the maximum power point and compare the tracking performance under a fair

number of iterations. In addition, since the actual application is an online continuous tracking process, the set number of iterations does not affect the tracking performance.

Table 2. Criteria for adjusting α and the slope of the P–V curve.

No \ Criterion	$s \triangleq \frac{P(t+1)-P(t)}{V(t+1)-V(t)}$	$\Delta P = P(t+1) - P(t)$ $\Delta P > 0$
1	$s > 2$	$\alpha = \Delta\alpha + 0.05$
2	$2 \geq s > 1.5$	$\alpha = \Delta\alpha + 0.03$
3	$1.5 \geq s > 1$	$\alpha = \Delta\alpha - 0.01$
4	$1 \geq s > 0.5$	$\alpha = \Delta\alpha - 0.03$
5	$0.5 \geq s > 0$	$\alpha = \Delta\alpha - 0.05$
6	$s = 0$	$\alpha = \Delta\alpha$
7	$0 > s \geq -0.5$	$\alpha = \Delta\alpha - 0.05$
8	$-0.5 > s \geq -1$	$\alpha = \Delta\alpha - 0.03$
9	$-1 > s \geq -1.5$	$\alpha = \Delta\alpha - 0.01$
10	$-1.5 > s \geq -2$	$\alpha = \Delta\alpha + 0.03$
11	$s < -2$	$\alpha = \Delta\alpha + 0.05$

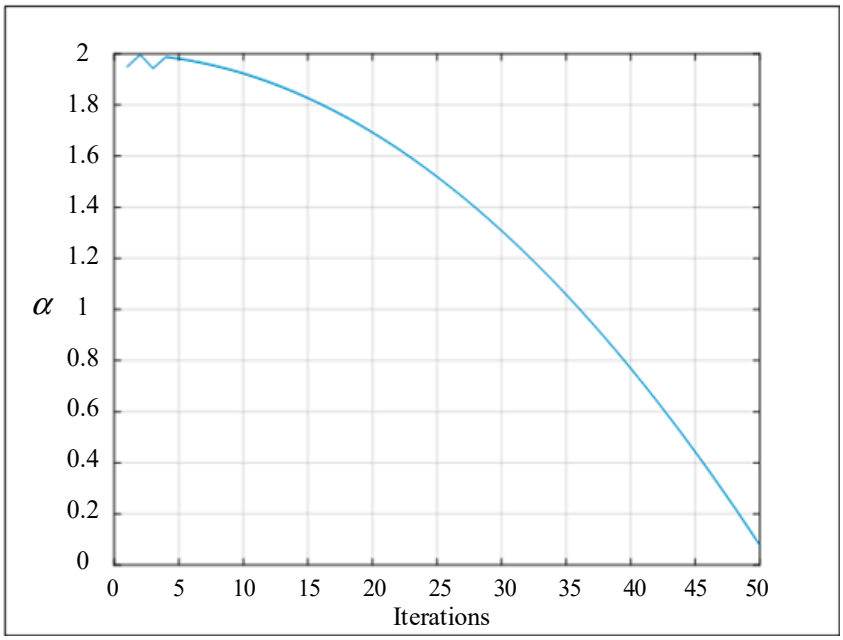

Figure 4. Trend of α with respect to the number of iterations.

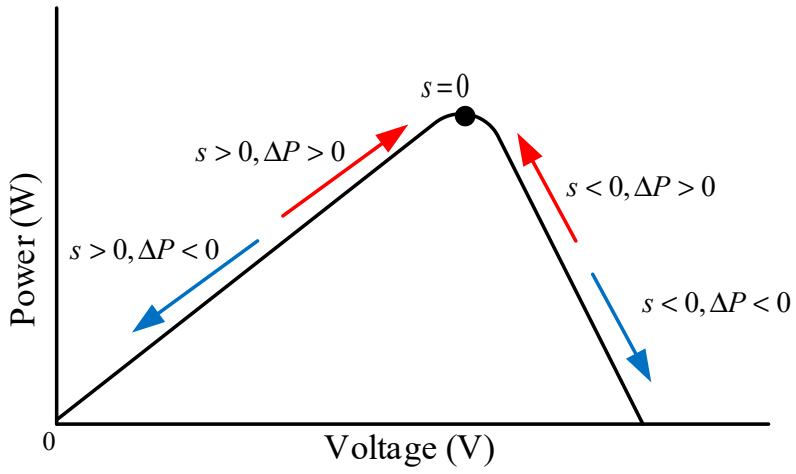

Figure 5. Relationship between the slope s of the P–V curve and changes in the PMA output power ΔP.

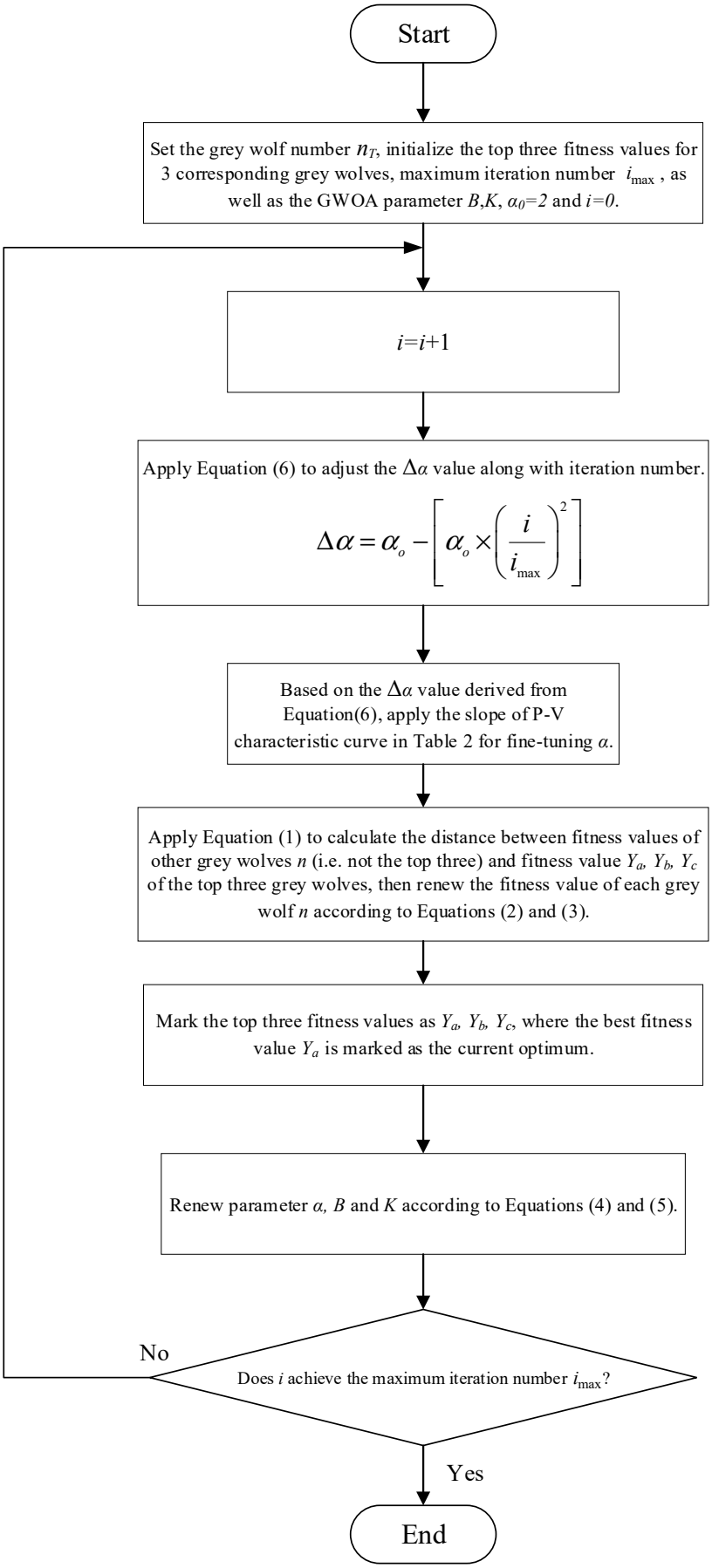

Figure 6. Iteration process of the modified GWOA.

4. High-Voltage Step-Up Converter

Figure 7 shows the circuit framework of the proposed high-voltage step-up converter. Its energy storage inductor is replaced by a coupled inductor, whose turns ratio increases the voltage conversion ratio. The proposed converter features a simple circuit framework and is easy to operate.

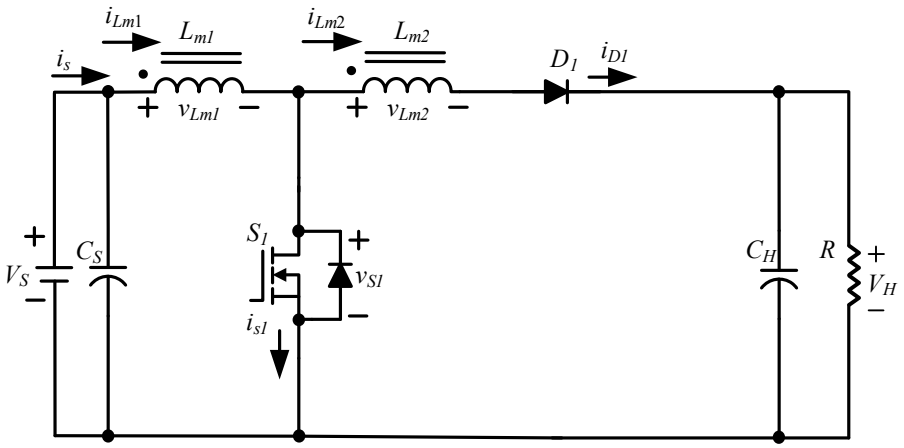

Figure 7. Circuit framework of the proposed high-voltage step-up converter.

4.1. Circuit Analysis of the High-Voltage Step-Up Converter

The proposed converter operates in two modes, depending on whether the switch is on or off. When the switch is on, the duty cycle D of the converter in period T is expressed as

$$D \triangleq \frac{t_{on}}{T} = \frac{t_{on}}{t_{on} + t_{off}} \tag{7}$$

where t_{on} is the amount of time during which the switch is on within a period, and t_{off} is the amount of time during which the switch is off within a period.

(1) Switch on ($0 \leq t_{on} \leq DT$)

When switch S_1 is on, diode D_1 is deactivated. The equivalent circuit of the converter is presented in Figure 8. Equation (8) defines the turns ratio N of the coupled inductor, Equations (9) and (10) define the inductance voltage v_{Lm1} and v_{Lm2}, respectively, and Equation (11) defines the voltage v_L at the two ends of the coupled inductor:

$$N \triangleq \frac{N_2}{N_1} \tag{8}$$

$$v_{Lm1} = V_S \tag{9}$$

$$v_{Lm2} = V_S \frac{N_2}{N_1} = V_S N \tag{10}$$

$$v_L \triangleq v_{Lm1} + v_{Lm2} = (1 + N) V_S \tag{11}$$

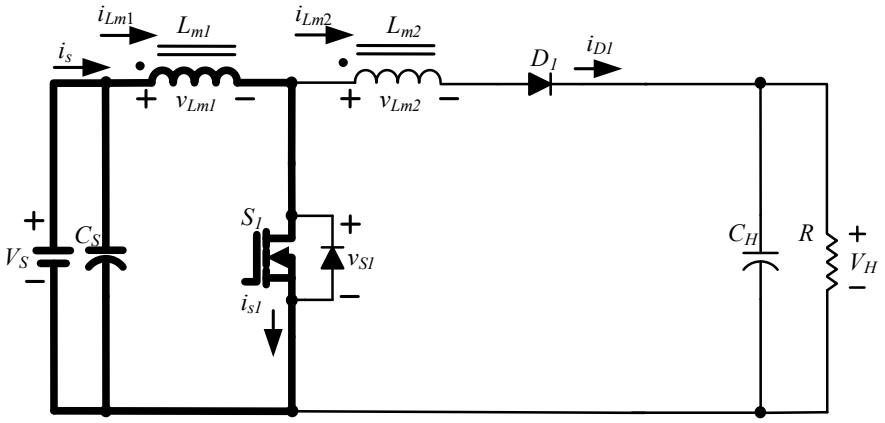

Figure 8. Equivalent circuit of the proposed high-voltage step-up converter when the main switch S_1 is on.

(2) Switch off ($DT \leq t_{off} \leq T$)

When switch S_1 is off, diode D_1 is activated. The equivalent circuit of the converter is presented in Figure 9. Equation (12) defines the voltage v_L at the two ends of the coupled inductor:

$$v_L = v_{Lm1} + v_{Lm2} = V_S - V_H \tag{12}$$

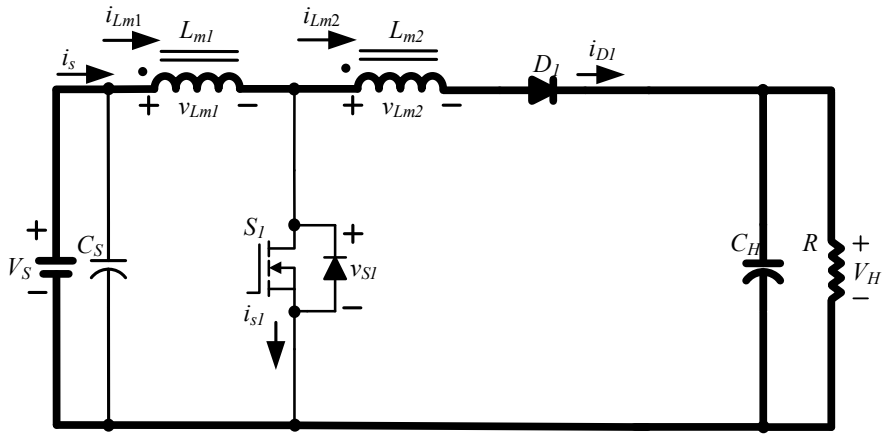

Figure 9. Equivalent circuit of the proposed high-voltage step-up converter when the main switch S_1 is off.

According to the volt–second balance law, Equation (13) is derived from Equations (11) and (12) and rearranged to Equation (14) to define the relationship between the output voltage V_H and input voltage V_S:

$$(1+N)V_S DT + (V_S - V_H)(1-D)T = 0 \tag{13}$$

$$\frac{V_H}{V_S} = \frac{(1+ND)}{(1-D)} \tag{14}$$

The relationship between the voltage gain and duty cycle is depicted in Figure 10. At the same duty cycle, the turns ratio of the coupled inductor increases the voltage conversion ratio of the step-up converter.

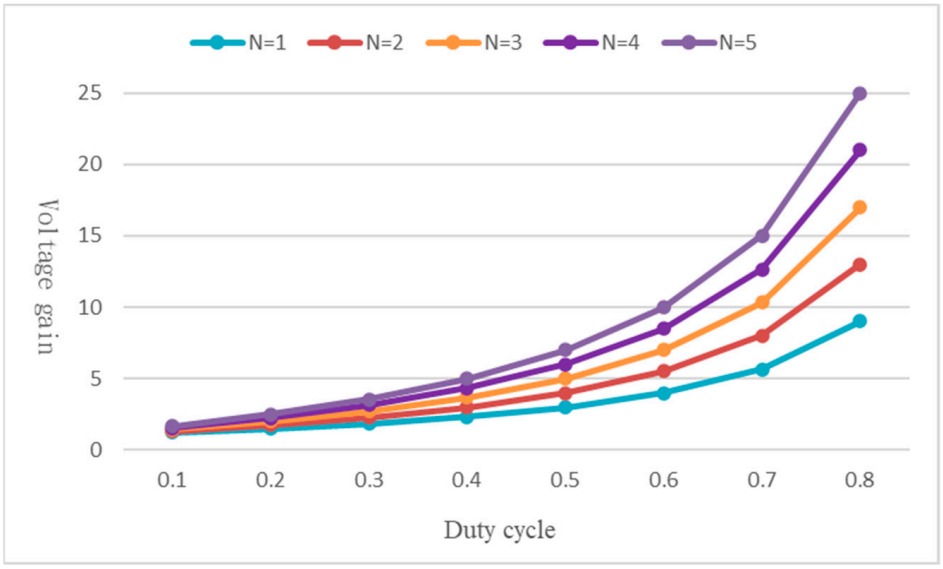

Figure 10. Relationship between the voltage gain and duty cycle of the high-voltage step-up converter.

4.2. Design of Converter Elements

Table 3 lists the electrical specifications of the proposed high-voltage step-up converter. The design of each converter element is described as follows.

Table 3. Electrical specifications of the proposed high-voltage step-up converter.

Parameter	Value
Low-voltage side direct input voltage (V_S)	V_S = 70 V ± 10%
High-voltage side direct output voltage (V_H)	V_H = 400 V
Switching frequency (f)	f = 25 kHz
Coupled inductor turns ratio (N)	$N = \frac{N_2}{N_1} = 2$
Rated output power (P)	P = 300 W

If each element is assumed to be ideal, then the input power P_{in} of the converter must be equal to the output power P_{out}:

$$V_S I_{Lm1} = \frac{{V_H}^2}{R} \tag{15}$$

Equations (14) and (15) are used to derive the mean excitation current passing through the primary side of the coupled inductor, as expressed in

$$I_{Lm1} = \frac{{V_H}^2}{V_S R} = \frac{{V_H}^2}{{V_S}^2}\frac{V_S}{R} = \left(\frac{1+ND}{1-D}\right)^2 \frac{V_S}{R} \tag{16}$$

where $\left(\frac{1+ND}{1-D}\right)$ is the voltage conversion ratio of the converter.

When the main switch S_1 is on, v_{Lm1} is expressed as

$$v_{Lm1} = V_S = L_{m1}\frac{di_{Lm1}}{dt} \tag{17}$$

According to Equation (17), when the inductor current linearly increases and the conduction time is less than $t_{on}(= DT)$, the increase in the inductor current $\Delta i_{Lm1(closed)}$ is expressed as

$$\Delta i_{L_{m1(closed)}} = \frac{V_S}{L_{m1}} DT \tag{18}$$

Therefore, the maximum and minimum inductor current values i_{Lm1} are calculated as follows [25]:

$$I_{Lm1(max)} = I_{L_{m1}} + \frac{\Delta i_{L_{m1}}}{2} = V_S \left[\left(\frac{1+ND}{1-D} \right)^2 \frac{1}{R} + \frac{D}{2L_{m1}f} \right] \tag{19}$$

$$I_{Lm1(min)} = I_{L_{m1}} - \frac{\Delta i_{Lm1}}{2} = V_S \left[\left(\frac{1+ND}{1-D} \right)^2 \frac{1}{R} - \frac{D}{2L_{m1}f} \right] \tag{20}$$

To ensure that the inductor current is in the continuous conduction mode (CCM), the minimum inductor current $I_{Lm1(min)}$ must be greater than 0. Therefore, Equation (20) is rearranged as follows:

$$V_S \left[\left(\frac{1+ND}{1-D} \right)^2 \frac{1}{R} - \frac{D}{2L_{m1}f} \right] \geq 0 \tag{21}$$

After Equation (21) is rearranged, the minimum excitation inductance on the primary side of the coupled inductor should meet the criterion of

$$L_{m1(min)} \geq \frac{D}{2f} \frac{(1-D)^2 R}{(1+ND)^2} \tag{22}$$

Because the framework of the coupled inductor is similar to that of an autotransformer, the maximum value of I_{Lm2} is calculated as follows [25]:

$$I_{Lm2(\max)} = \frac{-I_{Lm1(\max)}}{1+N} \tag{23}$$

4.3. Design of the Main Inductor Element

In this study, to ensure that the proposed high-voltage step-up converter operated in the CCM at full load (300 W), the rated load resistance of the converter was set to R = 533.3 Ω at a load voltage V_H and rated output power of 400 V and 300 W, respectively. According to Equation (22), when $\frac{dL_{m1}}{dD} = 0$, the largest inductance occurred when the duty cycle was 0.186. Therefore, according to Equation (22), L_{m1} was 698 μH. However, to ensure that the converter operated in the CCM, L_{m1} was multiplied by 1.25. Therefore, L_{m1} was set to 872 μH.

5. Simulation Results

MATLAB was used to simulate the MPPT of the PMA. The conventional P&O algorithm, conventional GWOA, and modified GWOA were used to track the MPP under different shading conditions, and the results were used to verify the effectiveness of the modified GWOA. PSIM was used to simulate the circuit of the proposed high-voltage step-up converter. Figure 11 depicts the steady-state response waveforms of the output voltage V_H, input voltage V_S, and duty cycle D with the converter operating at a load of P_L = 300 W. When the duty cycle was approximately 0.64, the input voltage of 70 V increased to the output voltage of 400 V. Therefore, the converter exhibited a high step-up ratio.

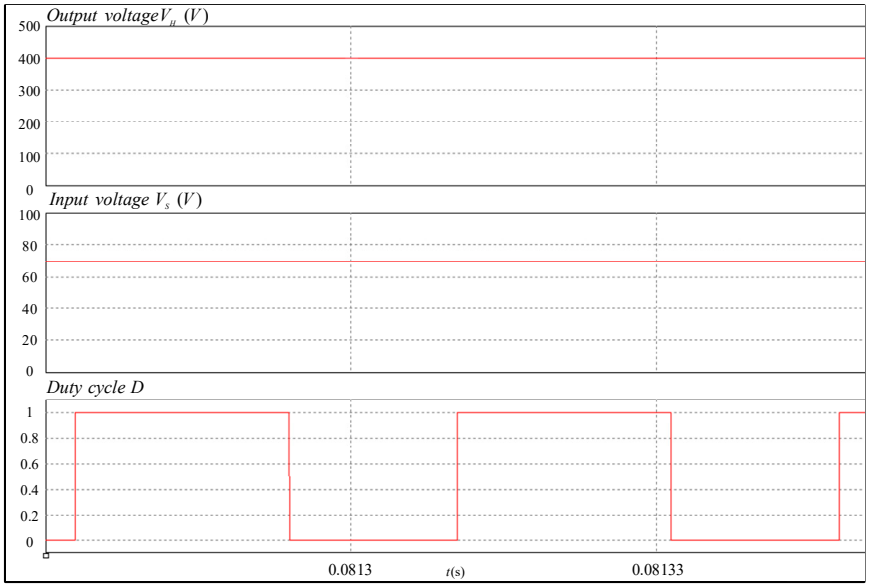

Figure 11. Steady-state response waveforms of the output voltage, input voltage, and duty cycle with the converter operating at a load of P_L = 300 W.

5.1. Simulation of the Modified GWOA

Table 4 presents the five cases of shading combinations used in this study. The number of peaks appearing on the P–V curve differs between the number of shaded modules and the percentage of the shaded area.

Table 4. Five cases of shading conditions.

Case	Module Connection and Shading Condition	Number of P–V Curve Peaks
1	Three parallel strings, with each string comprising four modules connected in series: (0% shading + 0% shading + 0% shading + 0% shading)// (0% shading + 0% shading + 0% shading + 0% shading)// (0% shading + 0% shading + 0% shading + 0% shading)	One

2	Three parallel strings, with each string comprising four modules connected in series:
	(0% shading + 0% shading + 0% shading + 50% shading)//
	(0% shading + 0% shading + 0% shading + 0% shading)//
	(0% shading + 0% shading + 0% shading + 0% shading)
		Two
		(MPP was on the right peak)

3	Three parallel strings, with each string comprising four modules connected in series:
	(0% shading + 0% shading + 30% shading + 90% shading)//
	(0% shading + 0% shading + 0% shading + 0% shading)//
	(0% shading + 0% shading + 0% shading + 0% shading)
		Three
		(MPP was on the middle peak)

4	Three parallel strings, with each string comprising four modules connected in series:
	(0% shading + 30% shading + 50% shading + 70% shading)//
	(0% shading + 0% shading + 0% shading + 0% shading)//
	(0% shading + 0% shading + 0% shading + 0% shading)
		Four
		(MPP was on the rightmost peak)

5	Three parallel strings, with each string comprising four modules connected in series: (0% shading + 10% shading + 80% shading + 90% shading)// (0% shading + 10% shading + 80% shading + 90% shading)// (0% shading + 10% shading + 80% shading + 90% shading)	Four (MPP was on the second peak from the left)

The parameters of both the conventional GWOA and the proposed modified GWOA are the same (i.e., $\alpha = \alpha_0 = 2$), the number of iterations is also set to 50, and the number of gray wolves is also set to 5. The only difference is that the proposed modified GWOA adopted Equation (6) and Table 2 to dynamically adjust the α parameter, while the conventional GWOA fixes the value of the α parameter to $\alpha = \alpha_0 = 2$.

5.1.1. Case 1

Figure 12 presents the P–V curve of Case 1, in which none of the modules was shaded. The maximum output power was 239.12 W. Figure 13 shows the MPPT results obtained using the conventional P&O algorithm, conventional GWOA, and modified GWOA. When only one peak appeared on the P–V curve, the three algorithms successfully tracked the MPP. However, compared with the other two algorithms, the modified GWOA exhibited a faster tracking speed response and steady-state response.

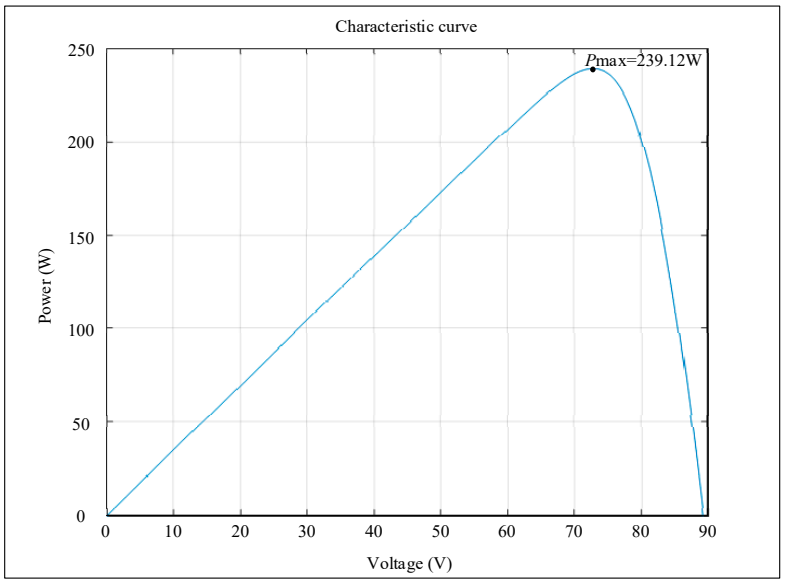

Figure 12. P–V curve of Case 1.

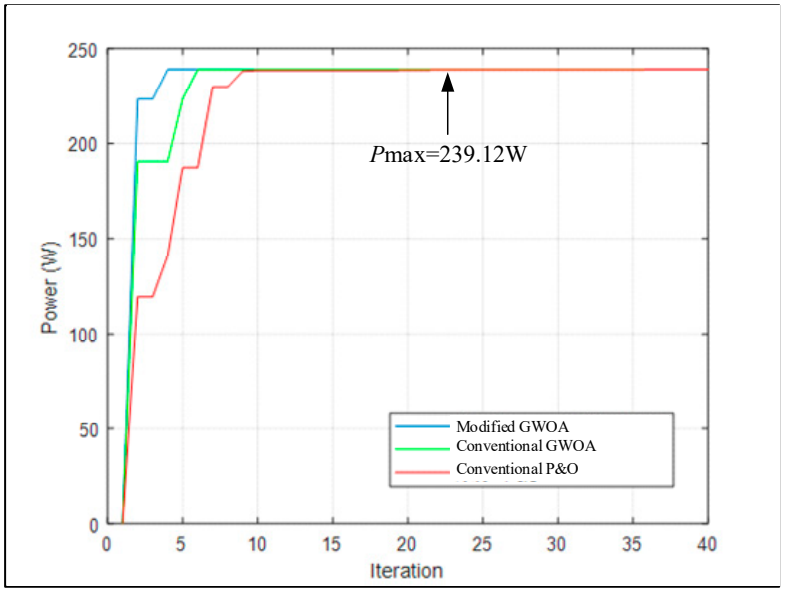

Figure 13. MPPT results of Case 1 obtained using the conventional P&O algorithm, conventional GWOA, and modified GWOA.

5.1.2. Case 2

Figure 14 presents the P–V curve of Case 2, in which a single module in the PMA was under 50% shading. Two peaks appeared on the curve, with the actual MPP located on the right peak. The maximum output power was 201.67 W. Figure 15 shows the MPPT results obtained using the conventional P&O algorithm, conventional GWOA, and modified GWOA. When two peaks appeared on the P–V curve, the conventional P&O algorithm and conventional GWOA became trapped in the local maxima for a short period, which compromised their tracking speed response. By contrast, the modified GWOA rapidly avoided the local maximum trap and thereby exhibited a fast tracking speed response.

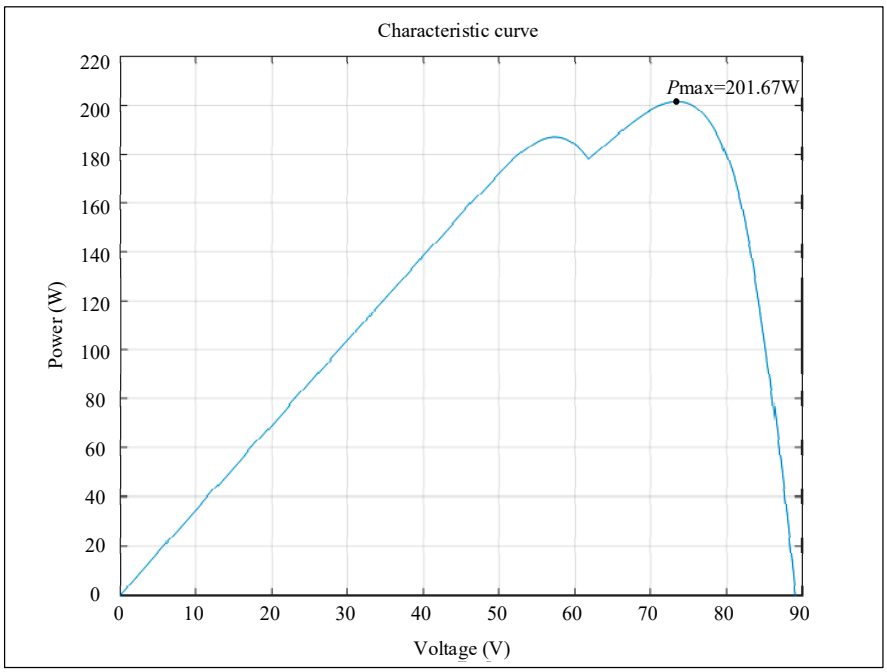

Figure 14. P–V curve of Case 2.

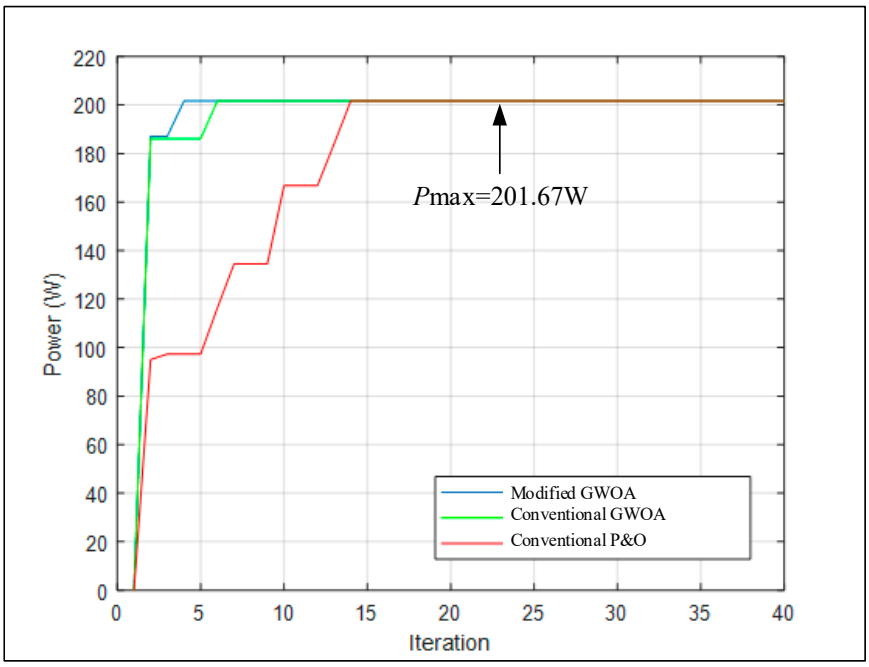

Figure 15. MPPT results of Case 2 obtained using the conventional P&O algorithm, conventional GWOA, and modified GWOA.

5.1.3. Case 3

Figure 16 presents the P–V curve of Case 3, in which one module was under 30% shading and another module was under 90% shading. Three peaks appeared on the curve, with the actual MPP located on the middle peak. The maximum output power was 178.93 W. Figure 17 shows the MPPT results obtained using the conventional P&O algorithm, conventional GWOA, and modified GWOA. Although the conventional P&O algorithm and conventional GWOA tracked the MPP, their tracking speed response and steady-state response were slower than those of the modified GWOA.

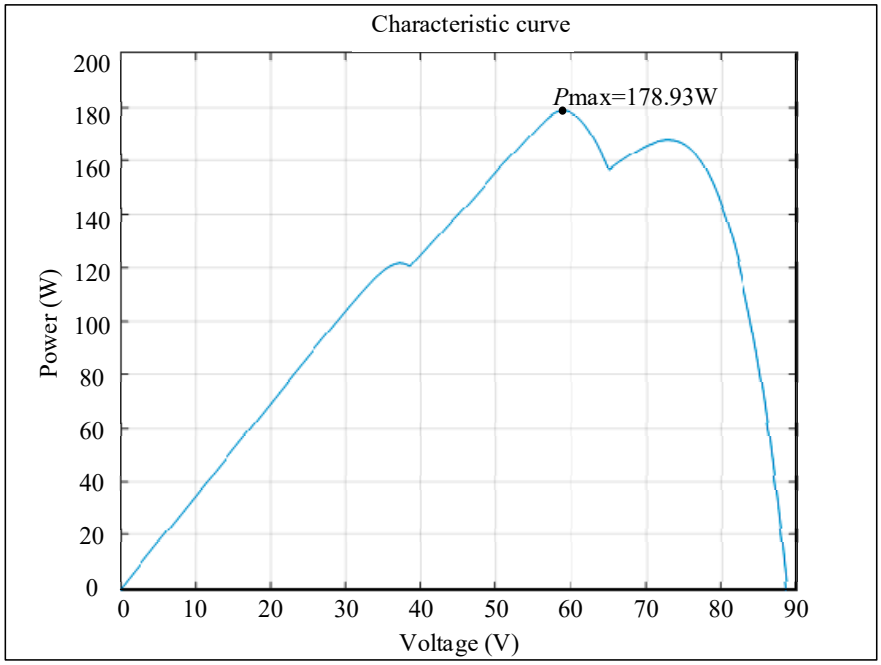

Figure 16. P–V curve of Case 3.

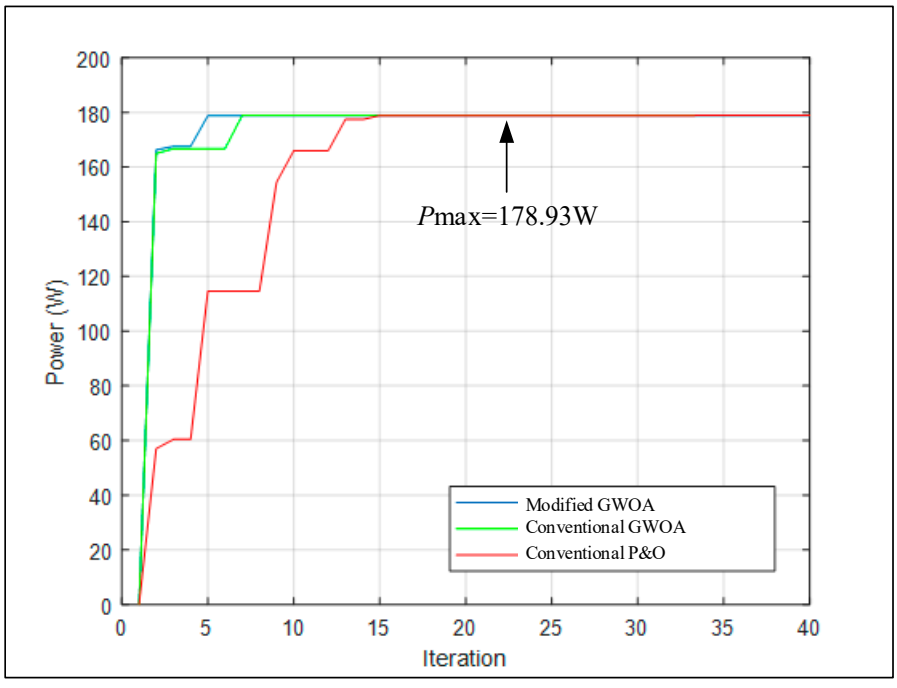

Figure 17. MPPT results of Case 3 obtained using the conventional P&O algorithm, conventional GWOA, and modified GWOA.

5.1.4. Case 4

Figure 18 presents the P–V curve of Case 4, in which three modules were under 30%, 50%, and 70% shading, respectively. Four peaks appeared on the curve, with the actual MPP located on the rightmost peak. The maximum output power was 184.72 W. Figure 19 shows the MPPT results obtained using the conventional P&O algorithm, conventional GWOA, and modified GWOA. Both the conventional P&O algorithm and the conventional GWOA were easily trapped in the local maxima, with the former being unable to identify the global maximum. By contrast, the tracking ability of the modified GWOA remained unaffected when four peaks appeared on the curve.

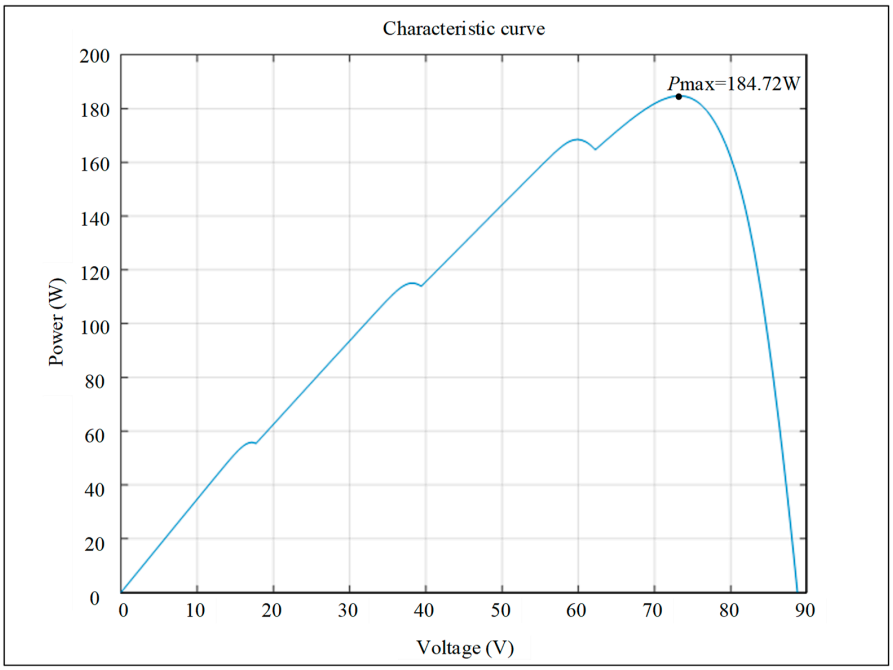

Figure 18. P–V curve of Case 4.

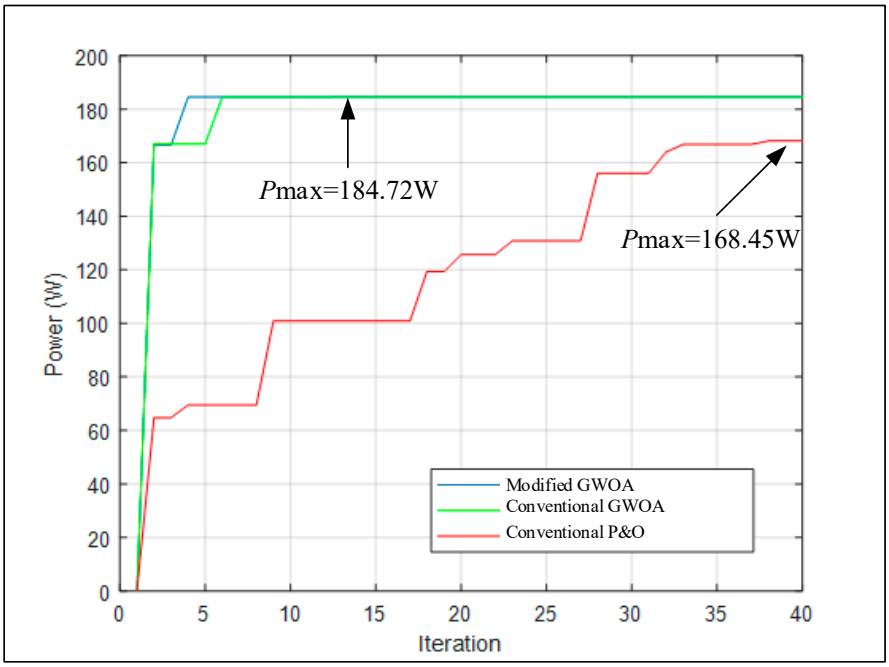

Figure 19. MPPT results of Case 4 obtained using the conventional P&O algorithm, conventional GWOA, and modified GWOA.

5.1.5. Case 5

Figure 20 presents the P–V curve of Case 5, in which three modules were under 10%, 80%, and 90% shading, respectively. Four peaks appeared on the curve, with the maximum MPP located on the second peak from the left. The maximum output power was 106.63 W. Figure 21 shows the MPPT results obtained using the conventional P&O algorithm, conventional GWOA, and modified GWOA. The modified GWOA not only accurately tracked the actual MPP but also exhibited a faster tracking speed response than those of the other two algorithms.

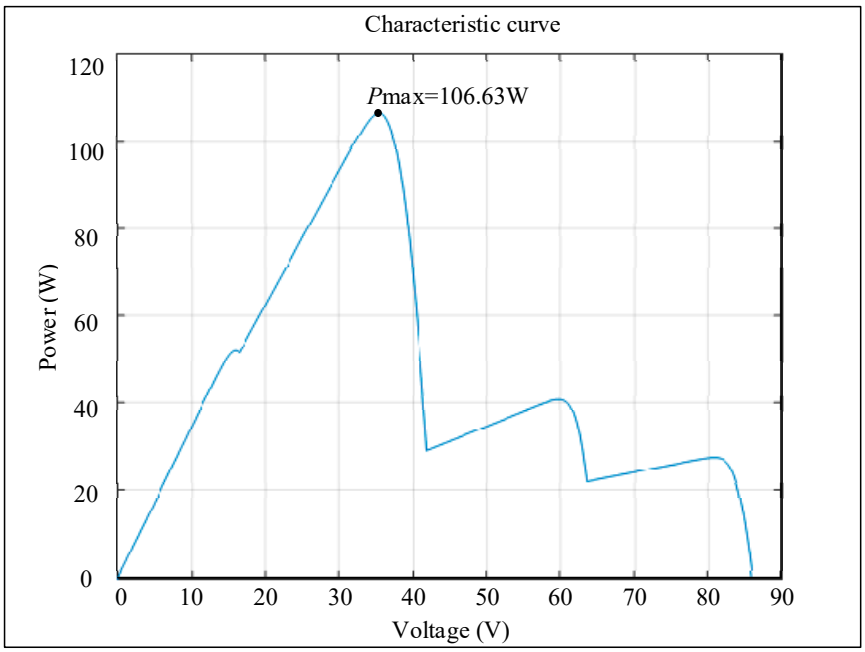

Figure 20. P–V curve of Case 5.

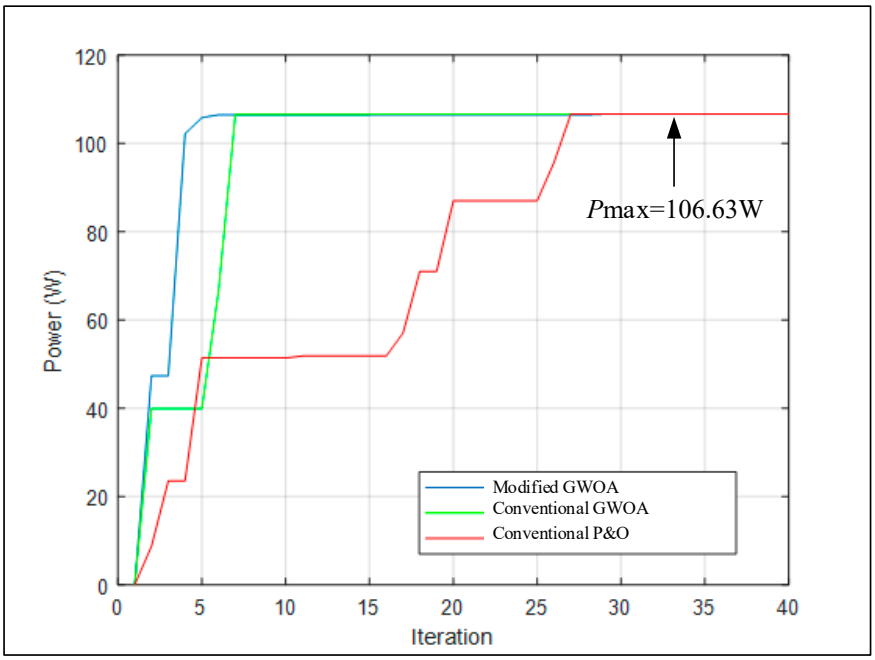

Figure 21. MPPT results of Case 5 obtained using the conventional P&O algorithm, conventional GWOA, and modified GWOA.

5.2. Comparison of Different Tracking Algorithms in Each Case

The conventional P&O algorithm, conventional GWOA, and modified GWOA were used to track the MPPs of the five cases. Each case was simulated 20 times. Table 5 presents the mean number of iterations required to track the MPP. Compared with the P&O algorithm and conventional GWOA, the modified GWOA required a smaller number of iterations to track the MPP.

Table 5. MPPT results of the five cases.

Case	Number of Peaks on the P–V Curve	Mean Iteration Number		
		Conventional P&O Algorithm	Conventional GWOA	Modified GWOA
1	One	11.4	8.6	7.5
2	Two (MPP on the right peak)	17.2	12.5	9.6
3	Three (MPP on the middle peak)	21.2	13.5	11.6
4	Four (MPP on the rightmost peak)	Failed	20.8	15.2
5	Four (MPP on the second peak from the left)	25.6	17.5	15.6

Take Case 1 as an example: from Figure 22, wherein the simulation results of maximum power point tracking adopted the conventional perturb and observe (P&O) method, the conventional GWOA, and the modified GWOA. If the area from the starting point of tracking to the global maximum power point (such as the black dashed line) is taken as the ideal output energy of the photovoltaic module array during the tracking process and the tracking curve of each method to the global maximum power point of the whole area is taken as the actual output energy, the ratio of the two is used to calculate the tracking efficiency. The tracking efficiency of the five cases adopting different methods is then listed in Table 6 for comparison. From Table 6, it can be observed that the tracking efficiency of the modified GWOA is the best among the three methods in different cases, while all of them were above 94.62%. In Case 4, the tracking efficiency was even as low as 36.73% because the conventional P&O method could not track the global maximum power point even after 50 iterations.

Table 6. Tracking efficiency comparison of the five cases.

Case	Number of Peaks on the P–V Curve	Tracking Efficiency (%)		
		Conventional P&O Algorithm	Conventional GWOA	Modified GWOA
1	One	76.46%	91.69%	98.15%
2	Two (MPP on the right peak)	68.84%	97.26%	98.48%
3	Three (MPP on the middle peak)	72.34%	97.41%	98.41%
4	Four (MPP on the rightmost peak)	36.73%	90.74%	94.85%
5	Four (MPP on the second peak from the left)	58.53%	88.43%	94.62%

The Introduction section has already described intelligent algorithms such as ant colony optimization (ACO) [5,6], artificial bee colony (ABC) algorithms [7,8], particle swarm optimization (PSO) [9,10], genetic algorithms (GAs) [11], teaching–learning-based optimization (TLBO) [12], cuckoo search-learning-based optimization algorithm (CSLBOA) [13–15],

as well as Bayesian optimization algorithm (BOA) [18]. Although they all have the ability to find the best solution in the global MPPT, one of the deficiencies identified is that their tracking response speed is still not fast enough. The main contribution of this paper is that when there are multiple peaks in the P–V characteristic curves due to shading of the photovoltaic module arrays, the maximum power point can be successfully tracked, and the proposed improved GWOA has better tracking speed response and stability than conventional intelligent algorithms. The five selected cases have been tested for different shading conditions with different peak numbers of P–V characteristics and tracking performance at different locations, and all of them exhibit better tracking performance, which should be representative and sufficient to prove the contributions of this proposed algorithm.

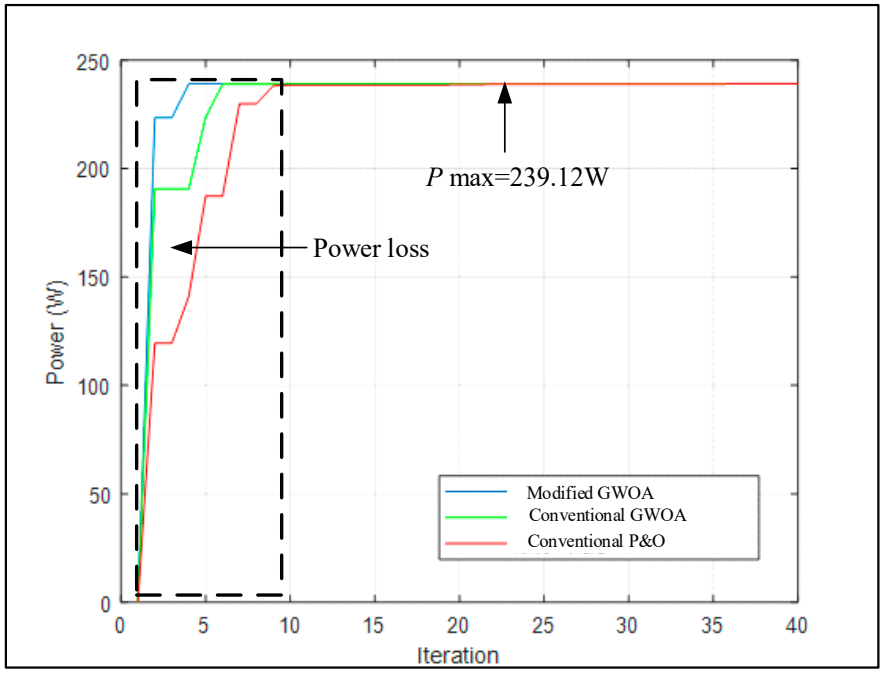

Figure 22. MPPT efficiency diagram of Case 1 obtained using the conventional P&O algorithm, conventional GWOA, and modified GWOA.

6. Conclusions

In this study, we proposed a modified GWOA by adjusting its iteration parameters to perform MPPT in PMAs. We used an MPP tracker composed of a high-voltage step-up converter. Overall, the proposed algorithm enables the online automatic adjustment of iteration parameters depending on the number of iterations and the slope of the P–V curve. According to our simulation results, when multiple peaks are present on the P–V curve of a PMA under different shading conditions, the modified GWOA remains unaffected and does not fall into the local maximum trap. It also exhibits a faster tracking speed response and steady-state response than those of the conventional P&O algorithm and conventional GWOA.

Author Contributions: K.-H.H. was in charge of project administration and completed the design of the high-voltage step-up converter. K.-H.C. planned the project and performed the writing, editing, and reviewing. Y.-P.K. completed the formal analysis of the improved gray wolf optimization algorithm. H.-H.C. conducted the software programming and simulation validation. All authors have read and agreed to the published version of the manuscript.

Funding: The authors gratefully acknowledge the support and funding of this project by the Ministry of Science and Technology, Taiwan, under Grant Number MOST 110-2221-E-167-067-MY2.

Data Availability Statement: This study did not report any data.

Conflicts of Interest: The authors declare no conflict of interest.

References

1. Sera, D.; Mathe, L.; Kerekes, T.; Spataru, S.V.; Teodorescu, R. On the Perturb-and-Observe and Incremental Conductance MPPT Methods for PV Systems. *IEEE J. Photovolt.* **2013**, *3*, 1070–1078. [CrossRef]
2. Ahmed, J.; Salam, Z. An Enhanced Adaptive P&O MPPT for Fast and Efficient Tracking under Varying Environmental Conditions. *IEEE Trans. Sustain. Energy* **2018**, *9*, 1487–1496.
3. Wang, J.; Yi, Y.; Yang, Y.; Zhang, G.; Huang, S. Research on Distributed Multi-peak Maximum Power Tracking Control. In Proceedings of the 29th Chinese Control and Decision Conference, Chongqing, China, 28–30 May 2017; pp. 2237–2341.
4. Ma, Y.; Zhou, X.; Gao, Z.; Bai, T. Summary of the Novel MPPT (Maximum Power Point Tracking) Algorithm Based on Few Intelligent Algorithms Specialized on Tracking the GMPP (Global Maximum Power Point) for Photovoltaic Systems under Partially Shaded Conditions. In Proceedings of the 2017 IEEE International Conference on Mechatronics and Automation (ICMA), Takamatsu, Japan, 6–9 August 2017; pp. 311–315.
5. Dorigo, M.; Birattari, M.; Stutzle, T. Ant Colony Optimization. *IEEE Comput. Intell. Mag.* **2006**, *1*, 28–39. [CrossRef]
6. Dhieb, Y.; Yaich, M.; Bouzguenda, M.; Ghariani, M. MPPT Optimization Using Ant Colony Algorithm: Solar PV Applications. In Proceedings of the IEEE 21st international Ccnference on Sciences and Techniques of Automatic Control and Computer Engineering (STA), Sousse, Tunisia, 19–21 December 2022; pp. 503–507.
7. Abdul, G.A.; Junita, M.S. Enhanced Global-Best Artificial Bee Colony Optimization Algorithm. In Proceedings of the Sixth UKSim/AMSS European Symposium on Computer Modeling and Simulation, Malta, Malta, 14–16 November 2012; pp. 95–100.
8. González, C.; Restrepo, C.; Kouro, S.; Rodriguez, J. MPPT Algorithm Based on Artificial Bee Colony for PV System. *IEEE Access* **2021**, *9*, 43121–43133. [CrossRef]
9. Pragallapati, N.; Sen, T.; Agarwal, V. Adaptive Velocity PSO for Global Maximum Power Control of a PV Array under Nonuniform Irradiation Conditions. *IEEE J. Photovolt.* **2017**, *7*, 624–639. [CrossRef]
10. Li, H.; Yang, D.; Su, W.; Lü, J.; Yu, X. An Overall Distribution Particle Swarm Optimization MPPT Algorithm for Photovoltaic System under Partial Shading. *IEEE Trans. Ind. Electron.* **2019**, *66*, 265–275. [CrossRef]
11. Megantoro, P.; Nugroho, Y.D.; Anggara, F.; Suhono; Rusadi, E.Y. Simulation and Characterization of Genetic Algorithm Implemented on MPPT for PV System under Partial Shading Condition. In Proceedings of the 2018 3rd International Conference on Information Technology, Information System and Electrical Engineering (ICITISEE), Yogyakarta, Indonesia, 13–14 November 2018; pp. 74–78.
12. Rao, R.V.; Savsani, V.J.; Vakharia, D.P. Teaching-learning-Based Optimization: A Novel Method for Constrained Mechanical Design Optimization Problems. *Comput. Aided Des.* **2011**, *43*, 303–315. [CrossRef]
13. Ahmed, J.; Salam, Z. A Soft Computing MPPT for PV System Based on Cuckoo Search Algorithm. In Proceedings of the 4th International Conference on Power Engineering, Energy and Electrical Drives, Istanbul, Turkey, 13–17 May 2013; pp. 558–562.
14. Soneji, H.; Sanghvi, R.C. Towards the Improvement of Cuckoo Search Algorithm. In Proceedings of the 2012 World Congress on Information and Communication Technologies, Trivandrum, India, 30 October–2 November 2012; pp. 878–883.
15. Nugraha, D.A.; Lian, K.L.; Suwarno. A Novel MPPT Method Based on Cuckoo Search Algorithm and Golden Section Search Algorithm for Partially Shaded PV System. *J. Elect. Comput. Eng.* **2019**, *42*, 173–182. [CrossRef]
16. Lian, K.L.; Jhang, J.H.; Tian, I.S. A Maximum Power Point Tracking Method Based on Perturb-and-Observe Combined with Particle Swarm Optimization. *IEEE J. Photovolt.* **2014**, *4*, 626–633. [CrossRef]
17. Daraban, S.; Petreus, D.; Morel, C. A Novel Global MPPT Based on Genetic Algorithms for Photovoltaic Systems under the Influence of Partial Shading. In Proceedings of the 39th Annual Conference of the IEEE Industrial Electronics Society, Vienna, Austria, 10–13 November 2013; pp. 1490–1495.
18. Zhang, Y.M.; ASCE, S.M.; Wang, H.; ASCE, M.; Mao, J.X.; Xu, Z.D.; Zhang, Y.F. Probabilistic Framework with Bayesian Optimization for Predicting Typhoon-induced Dynamic Responses of a Long-Span Bridge. *J. Struct. Eng.* **2021**, *147*, 04020297. [CrossRef]
19. Bollipo, R.B.; Mikkili, S.; Bonthagorla, K. Hybrid, Optimal, Intelligent and Classical PV MPPT Techniques: A Review. *CSEE J. Power Energy Syst.* **2021**, *7*, 9–33.
20. Atici, K.; Sefa, I.; Altin, N. Grey Wolf Optimization Based MPPT Algorithm for Solar PV System with SEPIC Converter. In Proceedings of the 4th International Conference on Power Electronics and their Applications (ICPEA), Elazig, Turkey, 25–27 September 2019; pp. 1–6.
21. Mohanty, S.; Subudhi, B.; Ray, P.K. A Grey Wolf Optimization Based MPPT for PV System under Changing Insolation Level. In Proceedings of the 2016 IEEE Students' Technology Symposium (TechSym), Kharagpur, India, 30 September–2 October 2016; pp. 175–179.
22. Subudhi, B.; Pradhan, R. A Comparative Study on Maximum Power Point Tracking Techniques for Photovoltaic Power Systems. *IEEE Trans. Sustain. Energy* **2013**, *4*, 89–98. [CrossRef]
23. Millah, I.S.; Chang, P.C.; Teshome, D.F.; Subroto, R.K.; Lian, K.L.; Lin, J. An Enhanced Grey Wolf Optimization Algorithm for Photovoltaic Maximum Power Point Tracking Control under Partial Shading Conditions. *IEEE J. Ind. Electron. Soc.* **2022**, *3*, 392–408. [CrossRef]

24. SunWorld Datasheet. Available online: http://www.ecosolarpanel.com/ecosovhu/products/18569387_0_0_1.html (accessed on 12 January 2023).
25. Narasimharaju, B.L.; Dubey, S.P.; Singh, S.P. Coupled Inductor Bidirectional DC-DC Converter for Improved Performance. In Proceedings of the 2010 International Conference on Industrial Electronics, Control and Robotics, Rourkela, India, 27–29 December 2010; pp. 27–29.